Nanoscale

PAPER

View Article Online
View Journal | View Issue

Check for updates

Cite this: *Nanoscale*, 2018, **10**, 20020

Precise synchronization of hyperthermia–chemotherapy: photothermally induced on-demand release from injectable hydrogels of gold nanocages†

Jiangshan Wan,‡[a,b] Shinan Geng,‡[a] Hao Zhao,‡[a] Xiaole Peng,[a] Jiabao Xu,[a] Meihe Wei,[a] Junxiong Mao,[a] Yang Zhou,[a] Quan Zhu,[b] Yanbing Zhao*[a] and Xiangliang Yang*[a]

Received 24th August 2018,
Accepted 28th September 2018

DOI: 10.1039/c8nr06851h

rsc.li/nanoscale

Though a therapeutic sequence plays a key role in tumor therapy, little attention has been paid to its influence on multimodal combined therapy. Herein, we developed gold nanocages (GNC@PNA-*hls*) decorated with two kinds of temperature sensitive p(*N*-isopropyl-acrylamide-acrylic acid) copolymers (PNA-*hs* and PNA-*ls*) for precise antitumor coordination of thermo-chemotherapy. Doxorubicin-loaded GNC@PNA-*hls* (Dox-GNC@PNA-*hls*) showed a steady photothermally induced on-demand release under multiple near-infrared (NIR) irradiations. *In vitro* evaluations indicated that concurrent thermo-chemotherapy treatments (Dox – L) showed the best antitumor effect, compared with the sequence of either doxorubicin treatment followed by NIR radiation (Dox + L) or NIR radiation followed by doxorubicin treatment (L + Dox). The *in vivo* antitumor efficacy also indicated that the tumor volume was totally suppressed (*ca.* 0.14 cm^3) by the treatment of Dox-GNC@PNA-*hls* with NIR radiation for 14 days. These results indicated that Dox-GNC@PNA-*hls* could achieve precise synchronization between hyperthermia and chemotherapy, and effectively enhance their antitumor efficacy.

Published on 02 tetor 2018. Downloaded by Fail Open on 7.5.2025 10:41:28 e paradites.

Introduction

Single-modality therapy for cancers, including surgery, chemotherapy and radiotherapy, has encountered increasingly serious challenges such as toxicity, drug tolerance, recurrence, metastasis *etc.*[1,2] Combined-modality therapies which involve a combination of many antitumor mechanisms have been developed clinically as the first-line therapy for most cancers in the past two decades.[3–5] Rational design of various antitumor strategies plays an important role in improving the therapeutic effect. For instance, it is well known that concurrent chemotherapy and/or radiotherapy treatment is emerging as a standard of care for treating many advanced cancers in clinical practice, owing to its superiority over the sequential strategy with significantly higher survival rates.[4–6] Recently, many studies on the combination therapies of hyperthermia and chemotherapy have also been reported to improve their antitumor efficacy.[6–9] Recently, thermotherapy has been receiving more and more attention in combined-modality therapies owing to its multiple tumoricidal mechanisms. For example, heat immediately destroyed cancer tissues/cells when the temperature increased above 50 °C, and this has been widely used as thermal ablation in the clinic.[10,11] Meanwhile, mild thermotherapy (hyperthermia, *ca.* 39–43 °C) greatly enhanced the antitumor efficacy of chemotherapeutic drugs by so-called thermo-sensitization including membrane damage, Na/K-ATP enzyme activation, injury of the DNA repairing protein, metabolic regulation of glutathione, the enhancement of blood perfusion and tumor penetration, *etc.*[12–16] As suggested by B. Hildebrandt and his coworkers, the thermal chemosensitization can yield the best results by synchronous application or administration of most chemotherapeutic drugs within a short interval (*e.g.* Dox and cisplatin).[17]

[a]*National Engineering Research Center for Nanomedicine, College of Life Science and Technology, Huazhong University of Science and Technology, Wuhan 430074, P. R. China. E-mail: zhaoyb@hust.edu.cn, yangxl@hust.edu.cn*
[b]*Institute of Consun Co. for Chinese Medicine in Kidney Diseases, Consun Pharmaceutical Group, Guangzhou 510530, P. R. China*

†Electronic supplementary information (ESI) available. See DOI: 10.1039/c8nr06851h

‡These authors contributed equally to this work and should be considered as co-first authors.

This journal is © The Royal Society of Chemistry 2018

Published on 02 tetor 2018. Downloaded by Fail Open on 7.5.2025 10:41:28 e paradites.

Though many heat sources (ultrasound, radio frequency, microwave, *etc*.) have been employed clinically, near-infrared (NIR) radiation has attracted more attention than other heat sources owing to its non-intrusive mode, good tissue penetration and no need for imaging guidance.[18–22] In most reports, coagulation necrosis of tumor tissues/cells usually occurred when these tissues/cells were heated above 50 °C using NIR photothermal therapy (NIR-PTT).[20–22] However, over-high temperatures might be inappropriate for thermo-sensitization of chemotherapeutic drugs. As reported by J. P. May,[23] the maximum synergistic interaction between hyperthermia and chemotherapy drugs often occurred at lower temperatures (*ca.* 39–43 °C). More importantly, it has been increasingly accepted that the synergistic interaction of heat with drugs was highly dependent on the operating sequence, interval times and types of drugs. Moreover, there is a consensus among clinicians that simultaneous treatments with multimodal therapies could achieve the best antitumor efficacy.[24–26] Unfortunately, it has been usually ignored in most studies on thermo-chemotherapy, and is often infeasible in clinic practice owing to the disparate tempos of action between drug release and NIR-PTT. That is, the action of the photothermal effect under NIR irradiation is pulsatile, quick and temporary, but the release and action of drugs are usually continuous, slow and long-term.

Some groups reported the synergistic antitumor effect of thermo-chemotherapy based on various NIR-PTT materials, including small molecules (ICG, Ce6, and DiR), polymers (PPy, PA, PEDOT: PSS, and PDA) and inorganic nanoparticles (gold, Pd, carbon, phosphorus, chalcogenide *etc.*).[27–35] In most of these studies, chemotherapeutic drugs were usually loaded by physical adsorption or chemical conjugation, and their release profiles were independent of NIR-PTT. This greatly limited the synergistic efficacy of these thermo-chemotherapies. In Y. N. Xia's recent work, temperature-sensitive pNIPAM modified gold nanocages (GNCs) were reported as smart drug delivery systems for NIR-triggered release of payloads.[28] Furthermore, hyaluronic acid modified GNCs were also used for achieving pinpointed intracellular drug release and targeting synergistic therapy.[33] However, NIR-PTT was often operated frequently according to therapeutic requirements against tumors. In this case, an on-demand drug release, which must be matched with multiple NIR-PTT therapies, played an important role in enhancing the antitumor outcomes of the multimodal combined therapy. Owing to the lack of sustained release and long-term intratumoral retention, unfortunately, it is still very difficult for these NIR-PTT drug delivery processes to achieve precise synchronization between hyperthermia and chemotherapy.

In order to solve the problem of the mis-match of the action timespan, nanomedicines with photothermally induced on-demand releasing characteristics are highly desired for achieving spatiotemporal management of photothermal-chemotherapy. Herein, two temperature sensitive poly(*N*-isopropylacrylamide-acrylic acid) (PNA) polymers with different lower critical solution temperatures (LCSTs) were modified successively on the surface of GNCs which possess hollow interiors and porous single-crystal walls and were synthesized *via* galvanic replacement of silver nanocubes (Fig. 1A and Fig. S1†).[36] Owing to the higher reaction activity of gold atoms near the pores of GNCs than those of other surface regions,[37] PNAs with a higher LCST (PNA-*h*s, *ca.* 39.9 °C) were firstly decorated on the surfaces near the pores of GNCs, and they served as temperature sensitive gated materials to switch on/off the drug release between the hyperthermia temperature (40 °C–45 °C) and body temperature (37 °C). The extended chains of PNA-*h*s made the GNC pores remain closed at body temperature, thus prohibiting the release of payloads from GNCs. When the temperature increased up to the LCST owing to the near-infrared-photothermal effect of GNCs, the PNA-*h* chains shrunk as a temperature sensitive coil–granule conformation transition occurred. This made the pores of GNCs open, and thus a rapid release of payloads from GNCs along with near-infrared-photothermal therapy (NIR-PTT) was achieved, that is, a precise synchronization of hyperthermia and chemotherapy resulted (Fig. 1B). In addition, PNAs with a lower LCST (PNA-*l*s, *ca.* 36.5 °C) were subsequently decorated on the surface regions away from the pores of GNCs, and this was responsible for realizing *in situ* gelation at body temperature. It improved the sustained release, long-term retention in tumor tissue and the synergistic effect of hyperthermia and chemotherapy.[38] The resultant temperature sensitive GNCs, which were decorated respectively with PNA-*h*s and PNA-*l*s onto different surface regions of GNCs, were named GNC@PNA-*hl*s.

Experimental

Materials

All materials were purchased from commercial suppliers and used without further purification, unless otherwise noted. *N*-Isopropylacrylamide (NIPAM, Tokyo Chemical Industry, Japan) was recrystallized from *n*-hexane. CuCl (Sinopharm Chemical Reagent Co., Ltd, China) was purified by dissolving it in concentrated hydrochloric acid and filtering off after dilution with water before use. *tert*-Butyl acrylate (*t*BA, purity > 99%, J&K, China), tris(2-dimethylaminoethyl)-amine (Me_6TREN, purity > 99.0%, Alfa Aesar), acetone (purity > 99.0%, Sinopharm Chemical Reagent Co., Ltd, China), bis[2-(2′-bromo-isobutyryloxy)-ethyl] disulfide (BiBOEDS, purity > 97.0%, Sigma-Aldrich, St Louis, USA) and Trifluoroacetic Acid (TFA, purity > 99.0%, Aladdin Reagent Co., Ltd, China) were used as received. HCl (37%) and chloroauric acid hydrate ($HAuCl_4{\cdot}4H_2O$, Au content > 47.8%) were purchased from Sinopharm Chemical Reagent Co., Ltd, China. Silver trifluoroacetate (CF_3COOAg, purity > 99.99%, Sigma Aldrich), ethylene glycol (EG, purity > 99.0%, Aladdin Reagent Co., Ltd, China), anhydrous sodium hydrosulfide (purity > 99%, Alfa Aesar), polyvinylpyrrolidone (PVP, M_w = 55 kDa, Sigma Aldrich), silver standard solution (1000 μg mL^{-1}, National Center of Analysis and Testing for Nonferrous Metals and Electronic Materials,

Published on 02 tetor 2018. Downloaded by Fail Open on 7.5.2025 10:41:28 e paradites.

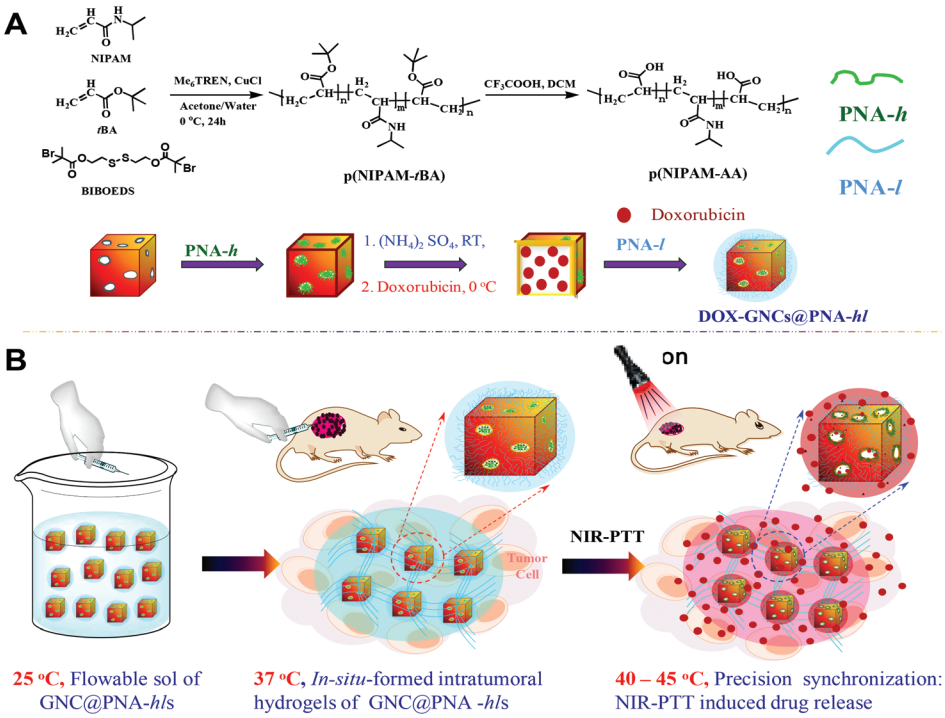

Fig. 1 The schematic diagrams of the synthetic route and the action principle of Dox-GNC@PNA-*hls*. (A) ATRP synthesis of PNA polymers, site-specific modification on GNCs and the remote drug-loading approach. (B) Temperature-sensitive sol–gel transition and precise synchronization of thermo-chemotherapy.

China) and gold standard solution (1000 μg mL^{-1}, National Center of Analysis and Testing for Nonferrous Metals and Electronic Materials, China) were used as received. Milli-Q ultrapure water (18.2 MΩ) was used in all experiments. All glassware used in the experiments was washed with an "aqua regia : water = 1 : 1" solution, and rinsed with ultrapure water and acetone twice respectively. All animal procedures were performed in accordance with the Guidelines for Care and Use of Laboratory Animals of the Science and Technology Department (Hubei Province, P. R. China) and approved by the Animal Ethics Committee of Huazhong University of Science and Technology.

Preparation of silver nanocubes and gold nanocages

Firstly, silver nanocubes (SNCs) were synthesized using a modified method reported before.[39] In brief, 50 mL of EG was first heated using an oil bath at 150 °C in a 250 mL round-bottomed flask for 30 min. Then sodium hydrosulfide in EG solution (3.0 mM, 0.6 mL), PVP in EG solution (20 mg mL^{-1}, 12.5 mL) and hydrochloric acid in EG solution (3.0 μmol mL^{-1}, 5 mL) were added into the flask under magnetic stirring. Afterwards, CF_3COOAg in EG solution (282 mmol L^{-1}, 4.0 mL) was quickly added to the solution while stirring. A series of color transitions from milky white, light yellow, red to tawny were observed in the synthesis process. The reaction was stopped by the addition of an ice/water mixture after 45 min. For removing excess EG and PVP, SNCs were purified by centrifugation (10 000 rpm × 10 min), washing with acetone once and ultrapure water twice, respectively. The refined SNCs were finally re-dispersed in 50 mL of ultrapure water, and stored at 4 °C for further use.

Using SNCs as a sacrificial template, gold nanocages (GNCs) were prepared using the galvanic replacement reaction.[32] In brief, SNCs (6.7 Ag mmol L^{-1}, 10 mL), PVP (55 kDa, 150 mg) and 90 mL of ultrapure water were added into a 250 mL three-necked flask, and the mixed solution was heated to 100 °C while stirring. Ten minutes later, a certain amount of $HAuCl_4$ solution (1.0 mmol L^{-1}) was added using a two-channel syringe pump (WZ-50C6, Zhejiang Smiths Medical Instrument Co, Ltd, China) at a 0.7 mL min^{-1} injection rate. A UV/Vis spectrophotometer (TU-1901, Beijing Purkinje General Instrument Co. Ltd, China) was used for monitoring the synthesis reaction. When the maximum absorption peak of the reaction system reached 808 nm, and herein its appearance was light blue, the addition of $HAuCl_4$ was ceased and the reaction solution was stirred for another 5 min at 100 °C. The resultant GNCs were purified by centrifugation (10 000 rpm × 10 min), washing with ammonium hydroxide once, absolute ethyl alcohol twice and ultrapure water twice, respectively. The refined GNCs were preserved at 4 °C for further use.

Synthesis of p(NIPAM-acrylic acid) (PNAs) with various LCSTs

Two kinds of PNA polymers, PNA-*ls* (their LCST was *ca.* 36.5 °C) and PNA-*hs* (their LCST was *ca.* 39–41 °C), were synthesized by atom transfer radical polymerization (ATRP).[40] Aiming to synthesize PNA-*ls* polymers which have a triblock architecture, for example, NIPAM (2.26 g, 20 mmol) was first

 This journal is © The Royal Society of Chemistry 2018

Published on 02 tetor 2018. Downloaded by Fail Open on 7.5.2025 10:41:28 e paradites.

dissolved in a mixed solution of acetone (8.0 mL) and H_2O (2.0 mL) in a Schlenk tube, while stirring at room temperature. The solution was degassed after freezing rapidly in liquid nitrogen. Subsequently, CuCl (20 mg, 0.2 mmol) and Me_6TREN (54 μL, 0.2 mmol) were quickly added at room temperature under an argon atmosphere. After performing a freeze–pump–thaw procedure two times as mentioned above, a degassed BiBOEDS solution (16 μL, 6.25 mmol mL^{-1}) was added into the solution at 0 °C under an argon atmosphere and stirred to initiate ATRP polymerization. The feeding molar ratio of NIPAM : Me_6TREN : BiBOEDS : CuCl was 200 : 2 : 1 : 2. A viscous PN polymer solution was obtained after 12 h of polymerization. Afterwards, degassed *t*BA (3.0 mL, 20 mmol) was added rapidly into the solution using a syringe. Triblock p(NIPAM-*b*-*t*BA) was obtained after another 18 h of polymerization under an argon atmosphere at 0 °C. After precipitation from water, dissolving in ethanol and dialyzing with ethanol/water (50/50 v/v), refined p(NIPAM-*b*-*t*BA) (*ca.* 1.0 g) was dissolved in 20 mL of dichloromethane. TFA (2.0 mL, 27 mmol) was rapidly added into the solution under stirring at 30 °C for the complete hydrolyzation of *t*BA into acrylic acid (AAc). In this case, the PNA-*l*2 polymer, in which the molar ratio of NIPAM/AAc was 200/200, was obtained after 12 h of TFA hydrolyzation. Similarly, PNA-*l*1 (its molar ratio of NIPAM/AAc was 200/100) was also synthesized using the same method.

The PNA-*hs* polymer, which was a random copolymer of NIPAM and acrylic acid, was also synthesized by a similar ATRP method. Taking the synthesis of PNA-*h*2 as an example, the molar ratio of NIPAM : *t*BA : Me_6TREN : BiBOEDS : CuCl was 400 : 8 : 2 : 1 : 2. In brief, NIPAM (2.26 g, 20 mmol) and *t*BA (58 μL, 0.4 mmol) were first dissolved in the mixed solution of acetone (8.0 mL) and H_2O (2.0 mL) in a Schlenk tube, while stirring at room temperature. After the solution was frozen rapidly in liquid nitrogen and degassed, CuCl (20 mg, 0.2 mmol) and Me_6TREN (54 μL, 0.2 mmol) were quickly added at room temperature under an argon atmosphere. After performing the freeze–pump–thaw procedure two times as mentioned above, degassed BiBOEDS solution (7.7 μL, 6.25 mmol mL^{-1}) was added into the solution at 0 °C to initiate ATRP polymerization. A random p(NIPAM-*co*-*t*BA) copolymer was obtained after another 18 h of polymerization under an argon atmosphere at 0 °C. The corresponding random PNA-*h* copolymers were obtained using the same method of TFA hydrolyzation as above. Random PNA-*h* polymers with various molar ratios of NIPAM/AAc, along with two triblock PNA-*l* polymers, are listed in Table 1.

Preparation of GNC@PNA-*hls*

Two temperature sensitive polymers with various LCSTs, PNA-*h* and PNA-*l*, were decorated in an orderly manner onto the surface of GNCs *via* a ligand exchange method, according to the difference of reaction activities between the surface near the pores of GNCs and the other surface. In brief, the GNCs (2.0 mg gold/10 mL water) were first washed three times with anhydrous alcohol (30 mL). After removing anhydrous alcohol by centrifugation (10 000 rpm × 15 min), the precipitated GNCs were re-dispersed in ultrapure water (*ca.* 10 mL), and were added dropwise to the PNA-*h*2 solution (50 mg mL^{-1}, 10 mL). The PVP polymers decorated onto the surface near the pores of GNCs were first substituted for PNA-*h*2, owing to higher reaction activities in these places than in other regions. In order to ensure the substitution of PNA-*h*2, the reaction system was stirred at 400 rpm for three days. After centrifuging (15 000 rpm × 15 min) the reaction system, the resultant precipitate, that is PNA-*h*2 locally decorated GNCs (GNC@PNA-*h*2), was washed with 2.0 mL of deionized water three times. Furthermore, purified GNC@PNA-*h*2 (1.0 mg gold/2.0 mL water) was added dropwise to a PNA-*l*1 solution (100 mg mL^{-1}, 2.0 mL) for achieving complete substitution of the remaining PVP decorated onto GNC@PNA-*h*2. The reaction system was stirred for 2 days. The resultant GNCs decorated with PNA-*h*2 and PNA-*l*1 were purified by the same centrifugation (15 000 rpm × 15 min) and deionized-water-washing (2.0 mL, 3 times), and was named GNC@PNA-*hl*s.

Characterization

The molecular compositions and structures of various PN*t*B and PNA polymers were characterized using a ^{1}H-NMR spectrometer (600 MHz, AV400, Bruker, Switzerland), and CD_3OD was used as a deuterated solvent. The molecular weights of PN*t*Bs and PNAs were measured by Gel Permeation Chromatography (GPC, Viscotek Malvern, England). The samples were dissolved

Table 1 The molecular compositions and structures of various PNA polymers

	M_n, kDa[a]			AAc/NIPAM[b]		
Polymer	Theo	Mea	PDI[a]	Theo	Mea	LCST, °C
PN (PN 400)	45.7	45.8	1.1	0	0	32
PNA-*h*1 (PNA 400-*co*-6)	48.8	41.0	1.09	0.015	0.015	33.7
PNA-*h*2 (PNA 400-*co*-8)	49.0	46.1	1.09	0.02	0.02	39.9
PNA-*h*3 (PNA 400-*co*-10)	49.2	45.3	1.11	0.025	0.026	>50
PNA-*l*1 (PNA 200-*b*-100)	36.8	37.5	1.09	0.50	0.5	36.5
PNA-*l*2 (PNA 200-*b*-200)	49.6	44.1	1.08	1.0	1.0	38.1

[a] Theoretical values (Theo) of number-average molecular weight (M_n) were calculated in term of the feeding ratio between monomer and initiator. The measuring values of M_n (Mea) and Polydispersitivity Index (PDI) were measured by GPC using polystyrene standards for calibration. [b] The molar ratio of both monomers (NIPAM and AAc). Theo was feeding ratio of the both monomers, and Mea was the measuring values of NIPAM and AAc amount in polymers using ^{1}H NMR.

Published on 02 tetor 2018. Downloaded by Fail Open on 7.5.2025 10:41:28 e paradites.

in tetrahydrofuran (THF) at a concentration of 5.0 mg mL^{-1}. Polystyrene (PS 99 K, M_w = 99 152 Da; M_n = 97 241 Da) and THF were used as standards and the mobile phase. The measurement conditions: the flow rate was 1.0 mL min^{-1} and the column temperature was 35 °C. The morphologies of GNCs and GNC@PNA-*hls* were characterized using a transmission electron microscope (TEM, 200 kV, Tecnai G2 20, FEI Corp., Netherlands), a high-resolution transmission electron microscope (HR-TEM, 300 kV, Tecnai G2 F30, FEI Corp, USA) and a field emission scanning electron microscope (FE-SEM, 10 kV, Sirion 200, FEI Corp, Netherlands). The samples were diluted to 20 μg mL^{-1} using ultrapure water. After ultrasonic oscillation for 10 minutes, 5 μL of the dilution was dropped onto a TEM copper grid (carbon film coated, 300-mesh), and dried at room temperature for TEM and HR-TEM characterization. In addition, a few drops of the samples were dropped onto a clean silicon slice, and dried using an infrared lamp for FE-SEM characterization. Thermogravimetric analysis (Diamond TG/DTA, PerkinElmer Instruments Co. Ltd, USA) of GNCs and GNC@PNA-*hls*, which were purified by centrifugation (15 000 rpm × 15 min, three times) and lyophilization, was performed in the temperature range from room temperature to 800 °C at 10 °C min^{-1} heating rate. The temperature sensitive transmittance values of various PNA-*h* and PNA-*l* polymers (2.0 mg mL^{-1}) were measured with a UV/Vis spectrophotometer (Lambda35, PerkinElmer Instruments Co. Ltd, USA) at a wavelength of 500 nm in the temperature range from 25 °C to 90 °C. The size and zeta potential of GNC@PNA-*hls* (0.01 mg mL^{-1}), which were ultrasonically oscillated for 5.0 min, were determined at room temperature using a dynamic light scattering instrument (DLS, ZetasizerNanoZS90, Malvern Instruments Ltd, UK) equipped with a 4 mW He–Ne laser source (λ = 633 nm) with a scattering angle of 90°.

Measurements of photothermal conversion efficiency

Aiming to measure the concentration-dependent photothermal conversion efficacy, 500 μL of GNC@PNA-*hls* dispersions with a series of concentrations (5, 10, 25, 50 and 100 μg mL^{-1}) were placed in a sealed quartz cuvette (4.5 × 1.0 × 0.5 cm) which was embedded in adiabatic foam, and irradiated at the wavelength of 808 nm for 10 min using an optical fibre coupled laser (MDL-808, the output power for continuous adjustment from 1 mW to 10 W, Changchun New Industries Optoelectronics Tech. Co., Ltd, China). At selected time intervals (30 s), the temperature of the sample dispersion was monitored using a near infrared thermal imager (FLIR-E64501, FLIR Systems Inc., USA). Water was used as the negative control under the same conditions. The photothermal conversion efficacy (η) was calculated according to the approach as reported before.[38]

$$\eta = \frac{hS(T_{max} - T_{surr}) - Q_{dis}}{I(1 - 10^{-A_{808}})} \times 100\% \quad (1)$$

where h is the heat transfer coefficient, S is the surface area of the container, T_{max} and T_{surr} are the equilibrium temperature and ambient temperature, respectively, Q_{dis} is measured using a quartz cuvette cell containing pure water, I is the incident laser power (0.4 W cm^{-2}), and A_{808} is the UV/Vis absorbance of GNC@PNA-*hls* at the wavelength of 808 nm.

Remote loading of doxorubicin into GNC@PNA-*hls*

The antitumor drug, doxorubicin, was loaded into GNC@PNA-*hls* *via* the so-called remote loading approach, which was applied in the drug-loading of Doxil® liposome as reported before.[42] In brief, GNC@PNA-*hls* dispersions (5.0 mg Au/5.0 mL) were incubated in an ammonium sulfate solution (0.2 mmol mL^{-1}, 5.0 mL) at room temperature for 12 h under stirring. After 30 min of ultrasonic oscillation, GNC@PNA-*hls* were centrifuged (15 000 rpm × 10 min) for removing the supernatant. 5.0 mL of a doxorubicin solution (2.0 mg mL^{-1}, 4 °C) was added dropwise to the resultant precipitate, while pipette blowing for the re-dispersion of GNC@PNA-*hls*. After another 12 h of incubation under stirring, doxorubicin-loaded GNC@PNA-*hls* (Dox-GNC@PNA-*hls*) were obtained by centrifugation (15 000 rpm × 10 min) and washed with ultrapure water three times. The drug loading (DL) amount and entrapment efficiency (EE) were calculated as follows (eqn (2) and (3)):

$$DL\% = \frac{W_0 - C_f V_f}{C_n V_n} \times 100\% \quad (2)$$

$$EE\% = \frac{W_0 - C_f V_f}{W_0} \times 100\% \quad (3)$$

where W_0 is the feeding amount of doxorubicin, C_f and V_f are the concentration and volume of free doxorubicin, respectively, and C_n and V_n are the concentration and volume of the GNC@ PNA-*hls* dispersions.

In vitro NIR-triggered on-demand release

In order to investigate the releasing behavior under NIR radiation, for example, 500 μL of various Dox-GNC@PNA-*hls* dispersions (100 μg mL^{-1} doxorubicin, 1.0 mg Au mL^{-1}) was added in a 2.0 mL EP tube, and then was irradiated with a NIR laser (λ = 808 nm, 5.0 min) at different powers. Afterwards, the dispersions were centrifuged (10 000 rpm × 10 min) and the supernatant was withdrawn at various time intervals. The residual precipitate was redispersed with 500 μL of deionized water for the next NIR radiation. The doxorubicin content of the supernatant was measured using a fluorescence spectrophotometer (F4500, Hitachi Co., Japan). The instrument parameters were as follows: λ_{ex} = 485 nm, λ_{em} = 554 nm and PMT voltage was 700 V. The accumulative release (AR at m times of NIR radiation) of doxorubicin was calculated as follows (eqn (4)):

$$AR = \frac{\sum_{i=1}^{m} C_i \cdot V_i}{\sum_{i=1}^{n} C_i \cdot V_i} \times 100\% \quad (4)$$

where C_i and V_i are the doxorubicin content and volume of the collected supernatant at NIR radiation of no. i, respectively.

 This journal is © The Royal Society of Chemistry 2018

Published on 02 tetor 2018. Downloaded by Fail Open on 7.5.2025 10:41:28 e paradites.

Temperature sensitive sol–gel phase transition behavior

Concentrated Dox-GNC@PNA-*hls* dispersions, which contained 100 μg mL^{-1} of doxorubicin, 1000 μg mL^{-1} of gold and 6.0–10 wt% of PNA polymers, were prepared for investigating temperature sensitive sol–gel phase transition *via* a vial inversion method in the temperature range from 10 °C to 50 °C. The samples were maintained for 10 min at each temperature point before determination. The dynamic viscoelastic properties of Dox-GNC@PNA-*hls* dispersions were measured using a stress-controlled rheometer (Kinexus ultra+, Malvern Instrument Ltd, UK) with a parallel plate (PP50, Φ = 50 mm, the gap was set at 0.5 mm) in the temperature range of 20 °C–50 °C. The measured parameters are as follows: the stress was 0.05 Pa, the heating rate was 1 °C min^{-1}, and the frequency was 1.0 Hz.

In vivo evaluation of antitumor activity

In vivo antitumor activities were evaluated in Balb/C mice (male, 20 ± 2 g) subcutaneously inoculated in the right flank with H22 cell suspensions (2.0×10^7 cells per 100 μL of saline). When the size of the solid tumor reached 150–200 mm^3 (approximately 7 mm in diameter), H22-bearing Balb/C mice were randomly divided into seven groups (n = 5 per group): (1) normal saline; (2) free Dox; (3) free Dox + laser; (4) GNC@PNA-*hls*; (5) GNC@PNA-*hls* + laser; (6) Dox-GNC@PNA-*hls*; and (7) Dox-GNC@PNA-*hls* + laser. Each group of mice received a single intratumoral injection of 50 μL of materials, and the concentrations of Dox and the gold element were 100 μg mL^{-1} and 1000 μg mL^{-1}, respectively. At 4 h after injection, the corresponding groups were specifically irradiated with NIR radiation (λ = 808 nm, 0.4 W cm^{-2}, 5 min). A NIR thermal imager was used to monitor the temperature of the tumor regions. The tumor volume was measured daily for the experimental period of 14 days, and calculated using the following formula: Volume = (length) × $(width)^2/2$.

In order to evaluate the precise synchronization of hyperthermia and chemotherapy of Dox-GNC@PNA-*hls*, 18 of the Balb/C mice (male, 20 ± 2.0 g) with subcutaneous tumors (150–200 mm^3) were randomly divided into 6 groups (n = 3). The mice of each group were injected intratumorally with 50 μL of administration dosage, and the treatments of each group are listed as follows: (1) a physical mixture of GNC@PNA-*hls* dispersions and 50 μg mL^{-1} of free Dox solution without NIR radiation; (2) a physical mixture of GNC@PNA-*hls* dispersions and 50 μg mL^{-1} of free Dox solution with NIR radiation; (3) a physical mixture of GNC@PNA-*hls* dispersions and 100 μg mL^{-1} of free Dox solution without NIR radiation; (4) a physical mixture of GNC@PNA-*hls* dispersions and 100 μg mL^{-1} of free Dox solution with NIR radiation; (5) Dox-GNC@GNC-*hls* (100 μg mL^{-1} of doxorubicin) without NIR radiation; and (6) Dox-GNC@GNC-*hls* (100 μg mL^{-1} of doxorubicin) with NIR radiation (λ = 808 nm, 0.4 W cm^{-2}, 5.0 min). In all treatment groups, the gold content was 1000 μg mL^{-1}, namely *ca.* 2.5 mg Au per kg body weight. NIR radiation conditions are listed as follows: λ = 808 nm, 0.4 W cm^{-2}, 5.0 min. The tumor volume was measured for 10 days, and the tumors were weighed to evaluate the influence of precise synchronization on the antitumor efficacy.

In vivo biodistribution of GNC@PNA-*hls*

The *in vivo* biodistribution of GNC@PNA-*hls* was investigated on H22-bearing Balb/C mice. GNC@PNA-*hls* dispersions (1000 μg mL^{-1}, 50 μL) were intratumorally injected into the mice when their tumor volume reached approximately 200 mm^3. The mice were sacrificed at different time intervals (1 h, and 1, 3, 5, 7, 10, and 14 days) after injection, and their tumor had been harvested for the measurement of the gold content. The tumor tissues were cut into small pieces, and mixed with the solution including concentrated HNO_3 (16 mol L^{-1}, 2.0 mL) and $HClO_4$ (12.4 mol L^{-1}, 0.5 mL). When the digestion was performed for *ca.* 0.5 h at 320 °C, 2 mL aqua regia was further added for achieving full digestion. When the digestive solution was concentrated to *ca.* 0.5 mL at 320 °C, it was diluted with deionized water to 5.0 mL for the measurement of the gold content with an atom absorption spectrophotometer (240FS, Agilent-Varian Co. Ltd, USA). A series of gold standard solutions (0.1, 0.25, 0.5, 1, 2.5, and 5 ppm) were prepared for obtaining a standard curve.

In vitro cytotoxicity assay

In order to evaluate the biocompatibility of GNC@PNA-*hls*, their *in vitro* cytotoxicity was determined on two cell lines (HepG2 and H22) using the MTT and Cell Counting Kit-8 (CCK8) methods, respectively. In brief, HepG2 and H22 cells were seeded in 96-well plates with DMEM and RPMI 1640 medium at the cell density of 1.0×10^5 cell per well respectively. After incubation overnight at 37 °C, they were further co-cultured with GNC@PNA-*hls* at various concentrations (0, 0.5, 1, 2.5, 5, 10, and 25 μg mL^{-1}) for 24 h. Afterwards, the cells were washed with PBS and then 20 μL of 3-(4,5-dimethylthiazol-2-yl)-2,5-diphenyltetrazolium bromide (MTT) (5.0 mg mL^{-1}) and/or 10 μL of the CCK-8 reagent (Dojindo China Co. Ltd, Japan) were added into each well, and the plates were incubated for an additional 4.0 h at 37 °C. The medium containing MTT was removed and 150 μL of DMSO was added to dissolve the resultant formazan crystals in living cells. DMEM/RPMI 1640 media with and without cells were used as the negative control and blank control, respectively. The optical density (OD) was measured at the wavelengths of 492 nm (for MTT assay) and 450 nm (for CCK8 assay) using a microplate reader (1420 multilabel counter, PerkinElmer, MA, USA). The cell viability was calculated using the following equation:

$$\mathrm{OD} = \frac{\mathrm{OD_s} - \mathrm{OD_b}}{\mathrm{OD_n} - \mathrm{OD_b}} \times 100\% \quad (5)$$

where OD_s, OD_b and OD_n are the OD values of the samples, blank control and negative control, respectively.

In order to compare the cytotoxicity under NIR radiation, HepG2 cells were plated at the cell density of 6000 cells per well in 96-well plates. After incubation for 12 h, they were co-

Published on 02 tetor 2018. Downloaded by Fail Open on 7.5.2025 10:41:28 e paradites.

cultured with various treatments including normal saline, free Dox solution, blank GNC@PNA-*hls* and Dox-GNC@PNA-*hls* (0.4 μg mL^{-1} Dox and 5.0 μg Au mL^{-1}) under NIR radiation (1.5 W cm^{-2}, 10 min), and the corresponding treatment without NIR radiation was used as the blank control. The cytotoxicity was assessed at 24 h post-treatment using a standard MTT method as mentioned above. In order to evaluate the influence of the action sequence of hyperthermia and chemotherapy on the antitumor efficacy, HepG2 cells were plated at a density of 10 000 cells per well in 96-well plates. After incubation for 12 h, the cells were divided into three groups based on various treatments: (1) the treatment of Dox + L: cells were incubated with a free Dox solution (1.0 μg mL^{-1}) for 12 h, and then NIR irradiation (1.0 W cm^{-2}, 5.0 min) was performed after blank GNC@PNA-*hls* (5.0 μg Au mL^{-1}) was added into the culture; (2) the treatment of L + Dox: NIR irradiation (1.0 W cm^{-2}, 5.0 min) was performed after blank GNC@PNA-*hls* (5.0 μg Au mL^{-1}) was added into the culture, and then a free Dox solution (1.0 μg mL^{-1}) was added to the cells and co-incubated for 12 h; (3) the treatment of L − Dox: GNC@PNA-*hls* (5.0 μg Au mL^{-1}) and a free Dox solution (1.0 μg mL^{-1}) were added into the culture, and simultaneous NIR irradiation (1.0 W cm^{-2}, 5.0 min) was performed before incubation at 37 °C for 12 h. Afterwards, the cells treated by the three modes were washed and incubated with fresh media for another 12 h. The standard MTT method was used to calculate their cell viabilities, as mentioned above. The cells were also observed using a confocal laser scanning microscope (Olympus IX81, Japan) and a flow cytometer (Beckman Coulter Cytomics FC500, USA) at the excitation wavelengths of 488 nm for calcein-AM and 559 nm for PI.

Statistical analysis

The data were expressed as mean ± SD. The measurement data were analyzed statistically by an independent-sample *t*-test and double-factor variance analysis, and the enumeration data were subjected to the chi-square (χ^2) test and Fisher's exact probability test. $p < 0.05$ was considered a statistically significant difference, and $p < 0.001$ was considered to be of high statistical significance.

Results and discussion

Preparation and characterization of GNC@PNA-*hls*

According to our precious work,[42–44] poly(*N*-isopropyl-acrylamide-*tert*-butyl acrylates) (PN*t*Bs) with various compositions and structures were synthesized by atom transfer radical polymerization, and then were hydrolyzed to PNA-*h*s and PNA-*l*s. The molecular compositions and structures of these polymers were verified by ^{1}H Nuclear Magnetic Resonance (^{1}H-NMR) and gel permeation chromatography (GPC) as shown in Table 1 and Fig. S2 and S3.† The dispersions of PNA-*h*s and PNA-*l*s exhibited distinct temperature dependence of light transmittance (Fig. S4†): as the copolymerizing amount of hydrophilic acrylic acid (AAc) increased from 1.5%, 2.0% to 2.5% in PNA-*h*s, the LCST increased from 33.7 °C (PNA-*h*1), 39.9 °C (PNA-*h*2) to above 50 °C (PNA-*h*3). In contrast to random copolymerization of PNA-*h*s, however, block copolymerization of PNA-*l*s seemed to have little influence on their LCSTs, which only increased from 36.5 °C to 38.1 °C when the amount of AAc in PNA-*l*s increased from 33.3% to 50.0%. More interestingly, the LCSTs of PNA-*h*s exhibited strong pH-dependence, while those of PNA-*l*s were not affected by the pH. For example, the LCST of PNA-*h*2 reduced from above 50 °C at pH 7.4 to *ca.* 39.9 °C at pH 6.5. Therefore, PNA-*h* could be used for switching on drug release at acidic tumor tissues at the hyperthermia temperature, and realizing precise synchronization between hyperthermia and chemotherapy. Meanwhile, PNA-*ls* exhibited robust temperature sensitivity at a broad pH range, which could be helpful in improving drug retention in the tumor. GNCs exhibited a uniform cubic shape with each side measuring about 50 nm, and some pores (*ca.* 3.0–5.0 nm) on the surface (Fig. 2, Fig. S5–S7†). After selective decoration of PNA-*h*s, the resultant GNC@PNA-*h*s showed lower element distributions of carbon and sulphur on the surface compared with GNC@PNA-*hls* (Fig. 2 B0–B3 *vs.* C0–C3). It meant that a selective decoration was accomplished by controlling the feeding sequence and the relative ratio of PNA-*h*/PNA-*l*. As reported by Z. H. Nie *et al.*,[45] sulfhydryl compounds selectively anchored to the {111} facets of gold nanoparticles. Therefore, a stoichiometric amount of PNA-*h* (50 mg per 2.0 mg GNC) was first decorated on the surface region near the pores of GNCs, which was mostly constituted by the {111} facets.[46] After PNA-*h*s completely covered the {111} facets of the GNC pores, excessive PNA-*l*s (100 mg per 2.0 mg GNC) was used to decorate the other GNC surfaces, which was mostly constituted by the {100} facets.

In addition, the modification of PNA-*h*s and PNA-*l*s had no effects on the properties of GNCs. As shown in Fig. S8A†, the UV/Vis absorption characteristic peaks were the same at *ca.*

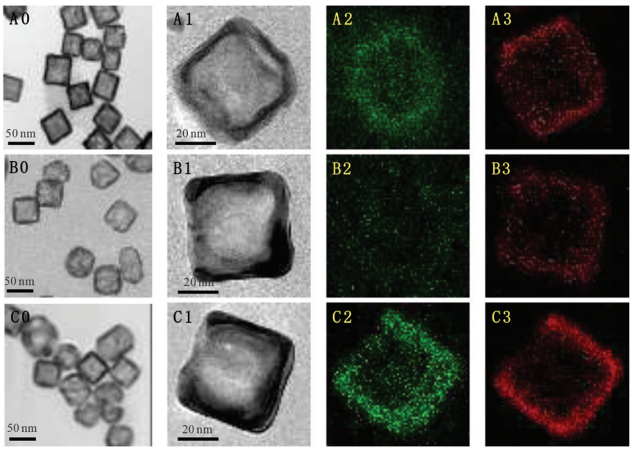

Fig. 2 The characterization of the microstructure and surface modification of GNCs (A0–A3), GNC@PNA-*h*s (B0–B3) and GNC@PNA-*hls* (C0–C3). Boxes 0, 1, 2, and 3 show TEM images (scale bar is 50 nm), high-resolution TEM images (scale bar is 20 nm), and the element distribution of carbon and sulphur, respectively.

This journal is © The Royal Society of Chemistry 2018

Published on 02 tetor 2018. Downloaded by Fail Open on 7.5.2025 10:41:28 e paradites.

790 nm, without any changes. Dynamic light scattering results indicated that the sizes of GNCs, GNC@PNA-*h*s and GNC@PNA-*hls* were in the range of 120–140 nm, and their zeta potentials gradually increased with the decorations of PNA-*h*s and PNA-*l*s, that is, they increased from −7.7 mV for GNCs to −17.8 mV for GNC@PNA-*h*s and −22.6 mV for GNC@PNA-*hls* (Fig. S8B–S8D†). The thermogravimetric analysis (TGA) indicated that GNC@PNA-*hls* suffered three kinds of weight losses in the temperature range between 20 °C and 700 °C (Fig. S9†). In contrast, pure GNCs (without PNA-*hls*) showed only one kind of weight loss (*ca.* 4.3 wt%) in the same temperature range, which could be attributed to the evaporation of water in the samples. The other two weight losses (*ca.* 10.5 wt% and 16.8 wt%) in the TGA curves of GNC@PNA-*hls* might be attributed to the pyrogenic decomposition of two components (NIPAM and AAc) in the PNA polymers.

In order to improve the drug-loading amount and sustained releasing behavior, the remote loading approach, which was firstly reported for Doxil liposomes,[41] was used in Dox-loading of GNC@PNA-*hls*. Based on the same principles, a high concentration of ammonium sulfate was first loaded into the inner cavity of GNC@PNA-*hls* (Fig. S10A†). Because of the "gate-keeper" role of PNA-*h*s, there existed a concentration gradient of ammonium sulfate between the inside and outside of GNCs, and it acted as the driving force for highly efficient loading of doxorubicin. When doxorubicin diffused into the cavities of GNCs through external PNA polymers, $(Dox)_2SO_4$ crystals were formed immediately and deposited in GNCs.[47] $(Dox)_2SO_4$-loaded GNC@PNA-*hls* are named Dox-GNC@PNA-*hls* henceforth in the present work. According to the approach, the drug loading amounts (DLs) of Dox-GNC@PNA-*hls*, with modification of PNA-*h*1, PNA-*h*2 or PNA-*h*3, reached up to 7.1–8.3% (Fig. S10B†).

Measurements of photothermal conversion efficiency

Compared to other photothermal materials (*e.g.* ICG, polypyrrole, gold nanorods or gold nanoshells), GNCs exhibit excellent NIR-PTT efficiency and high structural stability.[48,49] For example, the rising temperature (ΔT) of GNC@PNA-*hls* dispersions (100 μg mL^{-1} of gold content) reached 19 °C, 28 °C, and above 40 °C under NIR radiation (1.0 W cm^{-2}) for 3.0, 5.0 and 9.0 min, respectively. Even if the gold concentration was as low as 5.0 μg mL^{-1}, ΔT could also reach values higher than 10 °C under NIR radiation for 5.0 min. Given that the safe irradiation dose approved for clinical use by the FDA was no higher than 0.4 W cm^{-2},[50] the ΔT_s of GNC@PNA-*hls* dispersions still reached 10.9 °C for 3.0 min, and 22 °C for 9.0 min under 0.4 W cm^{-2} of NIR radiation (Fig. 3A). In addition, Fig. 3A also indicates that there is a strong positive correlation between the photothermal effect and the doxorubicin-releasing behavior of Dox-GNC@PNA-*hls*. Specifically for lower laser powers (0.4 W cm^{-2} and 1.0 W cm^{-2}), the near linear profiles of releasing kinetics indicated that zero-order release was achieved for Dox-GNC@PNA-*hls* by the NIR-induced photothermal effect. It was very beneficial for the precise synchronization of thermotherapy and chemotherapy.

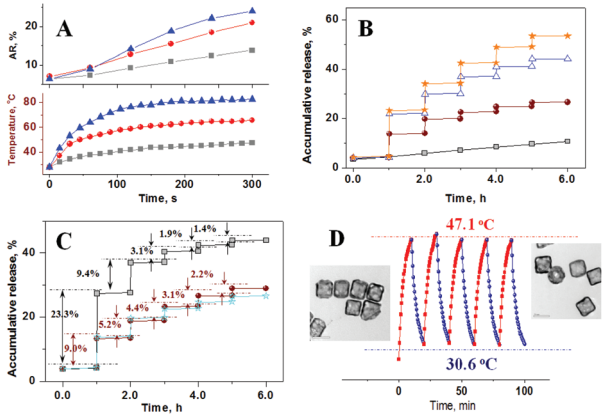

Fig. 3 *In vitro* evaluation of precise synchronization of thermo-chemotherapies. (A) Photothermal curves and corresponding thermally induced release of Dox-GNC@PNA-*hls* at various laser powers: 0.4 W (gray, square), 1.0 W (red, sphere), and 2.0 W (blue, triangle); (B) on-demand release of Dox from GNC@PNA-*hls* modified with various laser powers: 0 W (gray, square), 0.4 W (burgundy, sphere), 1.0 W (blue, star), and 2.0 W (cyan, star); (C) a comparison of the drug-releasing amounts of Dox-GNC@PNA-*hls* modified with various gatekeepers under multiple NIR irradiations: PN (black square), PNA-*h*2 (burgundy solid sphere), and PNA-*h*3 (cyan hollow star), 0.4 W cm^{-2}, 5.0 min; (D) heating and cooling curves of GNC@PNA-*hls* for five cycles of laser on/off; the left and right panels show the TEM images of GNC@PNA-*hls* before and after five cycles. Laser power density is 0.4 W cm^{-2}.

In vitro NIR-triggered on-demand release

Aiming to validate the precise synchronization, an on-demand release under multiple NIR irradiations at various laser powers was performed for Dox-GNC@PNA-*hls*. As shown in Fig. 3B, little doxorubicin was released from Dox-GNC@PNA-*hls* without NIR radiation, while a pulsed release of doxorubicin occurred immediately when NIR radiation was applied. The releasing amount of doxorubicin increased as the radiation power increased. That is, after performing 5.0 min of NIR irradiation five times, the accumulative releasing amounts reached 26.6%, 44.3% and 53.5% at 0.4 W cm^{-2}, 1.0 W cm^{-2} and 2.0 W cm^{-2}, respectively. The NIR-triggered on-demand release was highly dependent on the so-called "gate-keeper", that is the temperature sensitive PNA-*h*s which was modified on the pores of GNCs. When PNA-*h*s was replaced by PN (LCST = 32 °C),[51–53] for example, the accumulative releasing amount of doxorubicin prominently increased under NIR radiation. It was 23.3%, 9.4%, 3.1%, 1.9% and 1.4%, respectively, under five times NIR radiation, while the values were only 9.0%, 5.2%, 4.4%, 3.1% and 2.2% when either PNA-*h*2 (LCST = 39 °C) or PNA-*h*3 (LCST > 50 °C) was decorated as the gated material on GNCs (Fig. 3C). In order to simulate the clinical situations better, furthermore, the NIR-triggered release from Dox-GNC@PNA-*hls* was experimented for up to 8 days, and NIR irradiation (0.4 W cm^{-2}, 5.0 min) was performed once a day (Fig. S11†). The releasing amount of doxorubicin slightly decreased (8.7%, 7.3%, 7.3%, 5.3%, 4.2%, 3.8%, 3.1% and 2.2%) respectively in eight times of NIR-gating release. The

Published on 02 tetor 2018. Downloaded by Fail Open on 7.5.2025 10:41:28 e paradites.

multiple times and long-term of the on-demand release of Dox-GNC@PNA-*hls* by NIR irradiation were highly useful for the clinical application of the precise coordination between hyperthermia and chemotherapy. Furthermore, Fig. 3D indicates that GNC@PNA-*hls* exhibit uniform ΔT_s (from *ca.* 30 °C to 47 °C) under five times NIR-PTT irradiation. The high stability of the photothermal effect could be attributed to the excellent structural stability of GNC@PNA-*hls*, as demonstrated by the TEM images of GNC@PNA-*hls*. In contrast, most of the other photothermal materials, such as ICG and gold nanorods, rapidly lost their abilities on photothermal transduction, which resulted from the structure damage induced by repeated laser irradiation. According to the method reported by Roper *et al.*,[54] the photothermal conversion efficiency (η) of GNC@PNA-*hls* reached up to 39.1%, significantly higher than the η values of Au nanoshells (13%) and Au nanorods (21%).[55,56]

Long-term retention evaluation *in vivo*

The long-term retention of Dox-GNC@PNA-*hls* in tumors had great impact on their antitumor efficacies based on precise synchronization of hyperthermia and chemotherapy. Dox-GNC@PNA-*hls* exhibited a temperature sensitive sol–gel phase transition at 33.7 °C, which is close to the LCST of the PNA-*l* polymers. The storage modulus (G') and the loss modulus (G'') of Dox-GNC@PNA-*hls* increased from *ca.* 1.0 Pa and 0.2 Pa to *ca.* 2000 Pa and 75 Pa, respectively (Fig. 4A). Since PNA-*h* has a higher LCST (>39 °C) than body temperature, the temperature sensitive sol–gel transition of Dox-GNC@PNA-*hls* resulted apparently from the temperature sensitive coil–granule conformation transition of PNA-*ls* with their LCSTs (32 °C) being lower than body temperature. *In situ* gelation of GNC@PNA-*hls*, which resulted from the temperature sensitive sol–gel transition, greatly improved their long-term retention abilities in tumors. As shown in Fig. 4B, the retention amount of GNC@PNA-*hls* was always higher than that of free GNCs in tumor tissues, until 14 days post-treatment. Meanwhile, TEM images indicated that although there was no significant difference of the particle number with the treatments of GNC@PNA-*hls* and free GNCs during 5 days post-administration, a greater number of GNC particles were found with the treatment of GNC@PNA-*hls* than that of free GNCs at 10 days post-treatment (Fig. 4C). Therefore, GNC@PNA-*hls* exhibited a much stronger tumor-retention ability than free GNCs. It can be explained by the temperature sensitive sol–gel phase transition of PNA polymers at body temperature (37 °C), which significantly prolonged the retention time of GNC@PNA-*hls* in tumor tissues. The improvement of the tumor retention ability was advantageous in enhancing the antitumor efficacy of Dox-GNC@PNA-*hls*. The results were consistent with those reported before by us.[57–59]

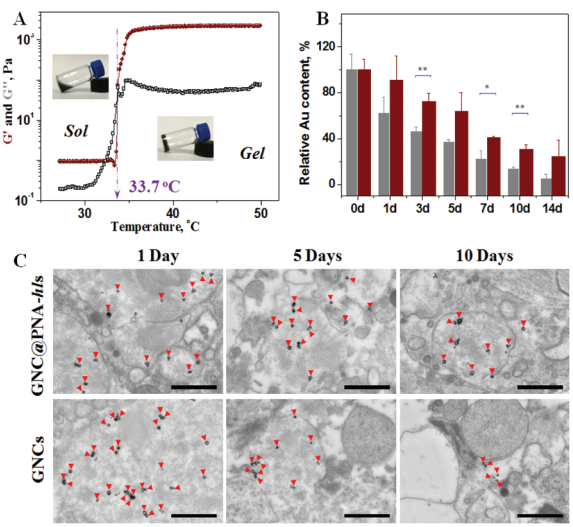

Fig. 4 *In vitro* and *in vivo* evaluations of the intratumoral retention behavior: (A) temperature sensitive sol–gel phase transition of Dox-GNC@PNA-*hls* dispersions by rheological measurements. The gray square and burgundy sphere are used to mark the storage modulus G' and the loss modulus G'', respectively. (B) Tumor retention comparison of the gold element after intratumoral administration of free GNCs (gray) and GNC@PNA-*hls* (burgundy). The dose of Dox and GNCs was 100 μg mL^{-1} and 1 mg mL^{-1}, respectively. (C) TEM images of tumor tissues after treatment with GNC@PNA-*hls* and free GNCs at 1, 5, and 10 days. The particles pointed by red arrows are GNCs. The bar is 1.0 μm.

In vitro evaluation of antitumor activity

In order to investigate the impact of NIR-triggered on-demand release of Dox-GNC@PNA-*hls* on the antitumor efficacy of combined therapies, the influence of treating sequences on the cytotoxicity of HepG2 cells was studied as shown in Fig. 5. Firstly, the cell viabilities after four treatments with control, free Dox, blank GNCs and Dox-GNC@PNA-*hls* with NIR radiation were compared, respectively, to those without NIR radiation. Clearly, no difference was found between treatments with and without NIR radiation in the groups of free Dox solution and control, while there were significant differences between with and without NIR radiation in both groups of blank GNC@PNA-*hls* and Dox-GNC@PNA-*hls* (Fig. 5A). Furthermore, Dox-GNC@PNA-*hls* showed higher cytotoxicity against HepG2 cells than blank GNC@PNA-*hls* groups under NIR radiation. It could be attributed to the precise synergistic interaction between the photothermal effect and NIR-triggered on-demand release of chemotherapeutic agents. We further studied how the treating sequence of chemotherapy and hyperthermia affected their antitumor efficacies. Fig. 5B shows that whether HepG2 cells were first incubated with a free Dox solution and subsequently subjected to NIR radiation (Dox + L) or were first subjected to NIR radiation and subsequently treated with the free Dox solution (L + Dox), their cell viabilities were much higher than those of concurrent treatments of Dox-GNC@PNA-*hls* and NIR radiation (Dox – L). This indicated that the best antitumor efficacy was achieved only when chemotherapy and hyperthermia were synchronized precisely. The fluorescence confocal images of HepG2 cells (Fig. 5C), which were co-stained with calcein-AM (green fluorescence for live cells) and propidium iodide (red fluorescence for dead

 This journal is © The Royal Society of Chemistry 2018

Published on 02 tetor 2018. Downloaded by Fail Open on 7.5.2025 10:41:28 e paradites.

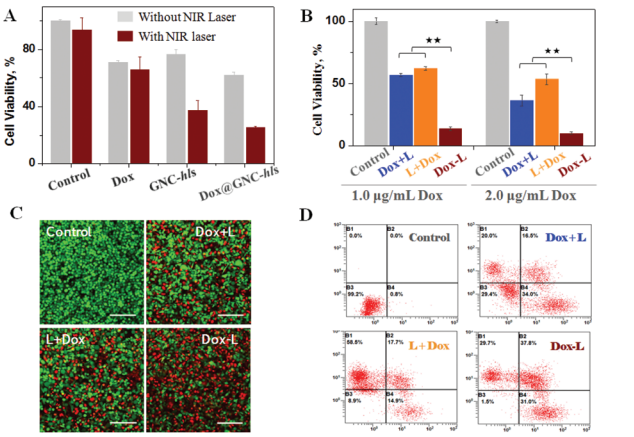

Fig. 5 *In vitro* evaluation of the precise synchronization of hyperthermia and chemotherapy of Dox-GNC@PNA-*hls*. (A) The cytotoxicity comparisons of control (normal saline), free Dox, GNC@PNA-*hls* and Dox-GNC@PNA-*hls* with and/or without NIR radiation (10 min, 1.5 W cm^{-2}). (B) The influence of the treating sequences on cytotoxicity. (C) Confocal microscopy image comparisons and relative fluorescence intensities of alive/dead cells after different treating sequences including Dox + L, L + Dox and Dox − L. The control is normal saline; the bar is 100 μm. (D) Flow cytometry analysis of cell apoptosis and necrosis in HepG2 cells after different treatments. Dox + L indicates a treating sequence in which tumor cells are first co-incubated with a Dox solution for 2 h, and then subjected to NIR radiation (5.0 min, 1.0 W cm^{-2}). L + Dox represents another treating sequence in which the tumor cells are first subjected to NIR radiation (5.0 min, 1.0 W cm^{-2}) and then co-incubated with the Dox solution for 2 h. Dox − L signifies the synchronized treatment of chemotherapy and NIR radiation, that is, tumor cells are co-incubated with the Dox solution for 2 h and NIR-irradiated for 5.0 min at 1.0 W cm^{-2} at the same time.

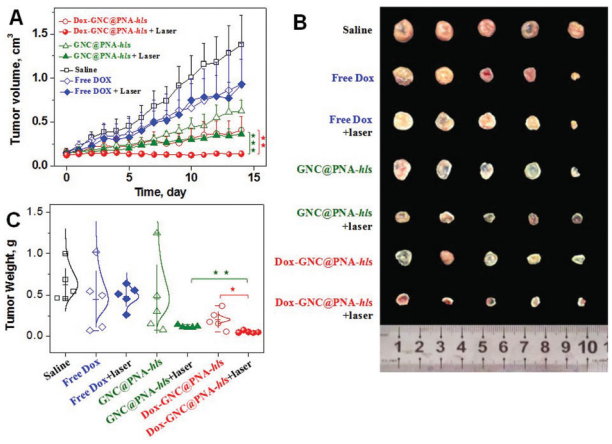

Fig. 6 *In vivo* comparison of the anti-tumor efficacy and the biodistribution in H22 tumor-bearing Balb/C mice subjected to various treatments. (A) Tumor growth curves. (B) The gross photos of tumor mass. (C) Tumor weight comparison for various treatments. Saline (black hollow square), free Dox solution without laser (green hollow diamond) and with laser (green solid diamond), GNCs without laser (blue hollow triangle) and with laser (blue solid triangle), and Dox-GNC@PNA-*hls* without laser (red hollow sphere) and with laser (red solid sphere).

cells), showed the highest intensity of red fluorescence and the lowest intensity of green fluorescence in the case of concurrent treatment (Dox − L) of thermo-chemotherapy among all treatments. An obvious difference in the relative fluorescence intensities was statistically found among the groups of Dox − L and Dox + L, or Dox − L and L + Dox. Similarly, the analysis using flow cytometry pointed out that the percentages of apoptotic cells were 0.8% for the blank group, 50.5% for the Dox + L group, 32.6% for the L + Dox group and 68.8% for the Dox − L group (Fig. 5D). All these results indicated that compared to either the Dox + L group or the L + Dox group, the concurrent thermo-chemotherapy treatment (Dox − L) achieved the best antitumor efficacy based on the NIR-radiation responsive on-demand release of the chemotherapeutic agent.

In vivo evaluation of antitumor activity

Furthermore, the precise synchronization of thermo-chemotherapy based on photothermally responsive on-demand release was investigated *via in vivo* antitumor evaluation on Balb/C mice (Fig. S12 and S13†). Dox-GNC@PNA-*hls* exhibited the best antitumor efficacy under NIR radiation, and was obviously better than the physical mixture of Dox solution and blank GNC@PNA-*hls* with the same concentration. Based on these results, the *in vivo* antitumor efficacy was first compared with or without NIR radiation (0.4 W cm^{-2}, 5.0 min) after a single dose of intratumoral injection into H22-tumor-bearing Balb/C mice, for confirming the potential benefits of Dox-GNC@PNA-*hls* on combined thermo-chemotherapy. As shown in Fig. 6A, Dox-GNC@PNA-*hls* under NIR radiation exhibited the most optimal antitumor effect against the H22 tumor. The tumor growth was totally suppressed (that is, the tumor volume always remained *ca.* 0.14 cm^3) when H22-tumor-bearing mice were treated with Dox-GNC@PNA-*hls* with NIR radiation once per 24 h for 14 days. In contrast, the tumor volume gradually increased from 0.37 cm^3 at the beginning to 0.14 cm^3 at the 14th day when the mice were treated with only Dox-GNC@PNA-*hls* without NIR radiation. There was a highly significant difference (three stars) in the tumor volumes at 14 days between treatments with Dox-GNC@PNA-*hls* both with and without NIR radiation. This difference between treatments with NIR radiation and no NIR radiation is visually shown in the gross photographs of excised tumors treated with Dox-GNC@PNA-*hls* and GNC@PNA-*hls* at the 14th day, and no difference is found in those treated with the free Dox solution (Fig. 6B). The weights of the excised tumors at the 14th day also indicated that Dox-GNC@PNA-*hls* under NIR radiation exhibited the best antitumor effect among all treatments. There were differences (at least one star) in tumor weights of the mice treated with Dox-GNC@PNA-*hls* under NIR radiation compared to those treated with either GNC@PNA-*hls* under NIR radiation or Dox-GNC@PNA-*hls* without NIR radiation (Fig. 6C).

These results clearly indicated that concurrent treatments of Dox-GNC@PNA-*hls* and NIR radiation achieved the best synergistic antitumor effect in all treatments. The photothermal effect from NIR radiation played an important role in the thermo-chemotherapy of Dox-GNC@PNA-*hls*. The tumor mass

Published on 02 tetor 2018. Downloaded by Fail Open on 7.5.2025 10:41:28 e paradites.

of mice treated with Dox-GNC@PNA-*hls* and GNC@PNA-*hls* exhibited a higher temperature (*ca.* 48 °C) than that of mice treated with the free Dox solution and saline (*ca.* 25 °C) under NIR radiation (Fig. S14†). In order to realize the photothermal conversion and on-demand release under many times of NIR irradiation for a long period, it had to be realized that gold nanocages stayed in the tumor mass and were not rapidly drained out. PNAs modified on GNCs, especially PNA-*l* polymers, played a key role in the long-term retention of GNCs in tumor mass. As shown in Fig. 4E, 53.8 ± 3.7% of injection dosage was lost for GNCs without surface modification of PNAs (naked GNCs) at 3 days, and only 27.4 ± 6.6% was lost for GNC@PNA-*hls* at the same time. There was even 24.7 ± 4.0% of injection dosage for GNC@PNA-*hls* at 14 days; meanwhile, only 4.8 ± 4.1% remained for naked GNCs at 14 days. The significant difference in the retention abilities in tumor could be reasonably attributed to the *in situ*-formed hydrogels of GNC@PNA-*hls*, which resulted from the temperature sensitive sol–gel phase transition of PNA-*l* polymers at body temperature.

Finally, we investigated the biocompatibility of Dox-GNC@PNA-*hls*. As shown in Fig. S15†, the cytotoxicities of Dox-GNC@PNA-*hls* were measured with two kinds of cells (HepG2 and H22 cells). It indicated that the viabilities of HepG2 cells measured by the MTT method were above 90% in the Au concentration range of 0–25 μg mL^{-1} for Dox-GNC@PNA-*hls* without NIR radiation. Meanwhile, the viabilities of H22 cells measured by the CCK8 assay were also above 90% in the Au concentration range of 0–5 μg mL^{-1}. In addition, the body weights of Balb/C mice were monitored in the animal test for antitumor evaluation (Fig. 6B). The data indicated that there was no difference in body weights among all treatments including control, free Dox, blank GNC@PNA-*hls* and Dox-GNC@PNA-*hls*, either with or without NIR irradiation.

Conclusions

In summary, two temperature sensitive polymers with different LCSTs, which served as gated materials to switch on/off drug release and *in situ* gelation systems, respectively, were used for the surface modification of GNCs. Moreover, the antitumor drug, doxorubicin, was fabricated efficiently as crystals into the chamber of GNCs *via* the so-called remote loading approach. The resultant Dox-GNC@PNA-*hls* showed NIR-radiation-responsive on-demand release. That is, little doxorubicin was released from Dox-GNC@PNA-*hls* without NIR radiation, since temperature sensitive PNA-*h* with a higher LCST (*ca.* 39.9 °C) acted as a gatekeeper which prevented the pre-leakage of drugs. As NIR radiation was applied on Dox-GNC@PNA-*hls*, a photothermal effect resulted from GNC induced temperature-sensitive phase transition of PNA-*h* from a swollen state into a shrunken state. Finally, the surface pores of GNCs, which were closed at body temperature by PNA-*h* polymers, were opened at the hyperthermia temperature (>40 °C), which enabled the release of doxorubicin loaded in GNCs under NIR radiation. For achieving homogeneous on-demand release induced by multiple NIR irradiations, PNA-*h*s (with LCSTs > 37 °C) were used as temperature sensitive gated polymers which were better than the polymers with lower LCSTs (<37 °C, *e.g.* PN). Meanwhile, temperature-sensitive *in situ* gelation at 37 °C, which arose from PNA-l polymers, also played an important role in on-demand sustained release and long-term retention of doxorubicin. Based on the NIR radiation responsive on-demand release, Dox-GNC@PNA-*hls* realized a precise synchronization of hyperthermia and chemotherapy. It was advantageous in improving the antitumor synergistic effect, since *in vitro* evaluation indicated that Dox-GNC@PNA-*hls* exhibit lower viabilities of cells under NIR radiation than a physical mixture of doxorubicin and GNC@PNA-*hls*. The best antitumor synergistic efficacy of Dox-GNC@PNA-*hls* from precise synchronization was also verified by *in vivo* antitumor evaluation on H22 tumor-bearing Balb/C mice. Along with their good biocompatibilities, Dox-GNC@PNA-*hls* could be hoped to be developed as new antitumor nanomedicines since it exhibited a precise synchronization of hyperthermia and chemotherapy based on NIR-radiation responsive on-demand release.

Conflicts of interest

There are no conflicts of interest to declare.

Acknowledgements

This work was supported by the National Natural Science Foundation of China (grant no. 81673016 and 81627901), the Key Fundamental Research Project from Shenzhen Research Council (2017)132, PCSIRT (IRT13016) and National Basic Research Program of China (2015CB931802). We also thank the Analysis and Test Center of HUST and School of Masters Engineering of HUST for related analysis.

References

1 H. B. El-Serag, *N. Engl. J. Med.*, 2011, **365**, 1118–1127.
2 Q. Chen, H. T. Ke, Z. F. Dai and Z. Liu, *Biomaterials*, 2015, **73**, 214–230.
3 Q. Y. Hu, W. J. Sun, C. Wang and Z. Gu, *Adv. Drug Delivery Rev.*, 2016, **98**, 19–34.
4 K. L. Nastiuk and J. J. Krolewski, *Adv. Drug Delivery Rev.*, 2016, **98**, 35–40.
5 S. Mura, J. Nicolas and P. Couvreur, *Nat. Mater.*, 2013, **12**, 991–1003.
6 R. X. Zhang, H. L. Wong, H. Y. Xue, J. Y. Eoh and X. Y. Wu, *J. Controlled Release*, 2016, **240**, 489–503.
7 A. Debes, R. Willers, U. Gobel and R. Wessalowski, *Pediatr. Blood Cancer*, 2005, **45**, 663–669.
8 W. Rao, Z. S. Deng and J. Liu, *Crit. Rev. Biomed. Eng.*, 2010, **38**, 101–116.

 This journal is © The Royal Society of Chemistry 2018

Published on 02 tetor 2018. Downloaded by Fail Open on 7.5.2025 10:41:28 e paradites.

9 C. L. Zhu, D. Huo, Q. S. Chen, J. J. Xue, S. Shen and Y. N. Xia, *Adv. Mater.*, 2017, **29**, 17034702(6).
10 E. S. Glazer and S. A. Curley, *Surg. Oncol. Clin. N. Am.*, 2011, **20**, 229–235.
11 P. Wust, B. Hildebrandt, G. Sreenivasa, B. Rau, J. Gellermann, H. Riess, R. Felix and P. M. Schlag, *Lancet Oncol.*, 2002, **3**, 487–497.
12 S. Lakshmanan, G. K. Gupta, P. Avci, R. Chandran, M. Sadasivam, A. E. S. Jorge and M. R. Hamblin, *Adv. Drug Delivery Rev.*, 2014, **71**, 98–114.
13 X. Jiang, S. Zhang, F. Ren, L. Chen, J. F. Zeng, M. Zhu, Z. X. Cheng, M. Y. Gao and Z. Li, *ACS Nano*, 2017, **11**, 5633–5645.
14 K. F. Chu and D. E. Dupuy, *Nat. Rev. Cancer*, 2014, **14**, 199–208.
15 N. Frazier and H. Ghandehari, *Biotechnol. Bioeng.*, 2015, **112**, 1967–1983.
16 A. J. Gormley, N. Larson, A. Banisadr, R. Robinson, N. Frazier, A. Ray and H. Ghandehari, *J. Controlled Release*, 2013, **166**, 130–138.
17 B. Hildebrandt, P. Wust, O. Ahlers, A. Dieing, G. Sreenivasa, T. Kerner, R. Felix and H. Riess, *Crit. Rev. Oncol. Hematol.*, 2002, **43**, 33–56.
18 W. Xiong, W. Wang, Y. Wang, Y. B. Zhao, H. B. Chen, H. B. Xu and X. L. Yang, *Colloids Surf., B*, 2011, **84**, 447–453.
19 N. Frazier, A. Payne, J. de Bever, C. Dillon, A. Panda, N. Subrahmanyam and H. Ghandehari, *J. Controlled Release*, 2016, **241**, 186–193.
20 L. C. Kennedy, L. R. Bickford, N. A. Lewinski, A. J. Coughlin, Y. Hu, E. S. Day, J. L. West and R. A. Drezek, *Small*, 2011, **7**, 169–183.
21 R. D. Issels, *Eur. J. Cancer*, 2008, **44**, 2546–2554.
22 D. Jaque, L. M. Maestro, B. del Rosal, P. Haro-Gonzalez, A. Benayas, J. L. Plaza, E. M. Rodriguez and J. G. Sole, *Nanoscale*, 2014, **6**, 9494–9530.
23 J. P. May and S. D. Li, *Expert Opin. Drug Delivery*, 2013, **10**, 511–527.
24 W. J. Curran, J. R. Paulus, C. J. Langer, R. Komaki, J. S. Lee, S. Hauser, B. Movsas, T. Wasserman, S. A. Rosenthal, E. Gore, M. Machtay, W. Sause and J. D. Cox, *J. Natl. Cancer Inst.*, 2011, **103**, 1452–1460.
25 Z. J. Zhou, A. Chan, Z. T. Wang, X. L. Huang, G. C. Yu, O. Jacobson, S. Wang, Y. J. Liu, L. L. Shan, Y. L. Dai, Z. Y. Shen, L. Lin, W. Chen and X. Y. Chen, *Angew. Chem., Int. Ed.*, 2018, **57**, 8463–8467.
26 X. H. Zheng, D. Xing, F. F. Zhou, B. Y. Wu and W. R. Chen, *Mol. Pharmaceutics*, 2011, **8**, 447–456.
27 H. Gong, L. Cheng, J. Xiang, H. Xu, L. Z. Feng, X. Z. Shi and Z. Liu, *Adv. Funct. Mater.*, 2013, **23**, 6059–6067.
28 Y. Wang, K. Y. Wang, R. Zhang, X. G. Liu, X. Y. Yan, J. X. Wang, E. Wagner and R. Q. Huang, *ACS Nano*, 2014, **8**, 7870–7879.
29 M. B. Zheng, C. X. Yue, Y. F. Ma, P. Gong, P. F. Zhao, C. F. Zheng, Z. H. Sheng, P. F. Zhang, Z. H. Wang and L. T. Cai, *ACS Nano*, 2013, **7**, 2056–2067.
30 L. Cheng, C. Wang, L. Z. Feng, K. Yang and Z. Liu, *Chem. Rev.*, 2014, **114**, 10869–10939.
31 M. S. Yavuz, Y. Y. Cheng, J. Y. Chen, C. M. Cobley, Q. Zhang, M. Rycenga, J. W. Xie, C. Kim, K. H. Song, A. G. Schwartz, L. H. V. Wang and Y. N. Xia, *Nat. Mater.*, 2009, **8**, 935–939.
32 Z. Z. Wang, Z. W. Chen, Z. Liu, P. Shi, K. Dong, E. G. Ju, J. S. Ren and X. G. Qu, *Biomaterials*, 2014, **35**, 9678–9688.
33 J. Y. Chen, M. X. Yang, Q. A. Zhang, E. C. Cho, C. M. Cobley, C. Kim, C. Glaus, L. H. V. Wang, M. J. Welch and Y. N. Xia, *Adv. Funct. Mater.*, 2010, **20**, 3684–3694.
34 Y. N. Xia, W. Y. Li, C. M. Cobley, J. Y. Chen, X. H. Xia, Q. Zhang, M. X. Yang, E. C. Cho and P. K. Brown, *Acc. Chem. Res.*, 2011, **44**, 914–924.
35 S. E. Skrabalak, L. Au, X. D. Li and Y. N. Xia, *Nat. Protoc.*, 2007, **2**, 2182–2190.
36 Z. H. Nie, D. Fava, M. Rubinstein and E. Kumacheva, *J. Am. Chem. Soc.*, 2008, **130**, 3683–3689.
37 R. T. Xing, K. Liu, T. F. Jiao, N. Zhang, K. Ma, R. Y. Zhang, Q. L. Zou, G. H. Ma and X. H. Yan, *Adv. Mater.*, 2016, **28**, 3669–3676.
38 Q. A. Zhang, W. Y. Li, L. P. Wen, J. Y. Chen and Y. N. Xia, *Chem. – Eur. J.*, 2010, **16**, 10234–10239.
39 J. D. Ye and R. Narain, *J. Phys. Chem. B*, 2009, **113**, 676–681.
40 Q. W. Tian, F. R. Jiang, R. J. Zou, Q. Liu, Z. G. Chen, M. F. Zhu, S. P. Yang, J. L. Wang, J. H. Wang and J. Q. Hu, *ACS Nano*, 2011, **5**, 9761–9771.
41 Y. Barenholz, *J. Controlled Release*, 2012, **160**, 117–134.
42 J. S. Wan, S. N. Geng, H. Zhao, X. L. Peng, Q. Zhou, H. Li, M. He, Y. B. Zhao, X. L. Yang and H. B. Xu, *J. Controlled Release*, 2016, **235**, 328–336.
43 Y. M. Liu, X. L. Peng, K. Qian, Y. Y. Ma, J. S. Wan, H. Li, H. S. Zhang, G. F. Zhou, B. Xiong, Y. B. Zhao, C. S. Zheng and X. L. Yang, *J. Mater. Chem. B*, 2017, **5**, 907–916.
44 H. Zhao, J. B. Xu, J. S. Wan, S. A. Geng, H. Li, X. L. Peng, Q. W. Fu, M. He, Y. B. Zhao and X. L. Yang, *Nanoscale*, 2017, **9**, 5859–5871.
45 Z. H. Nie, D. Fava, E. Kumacheva, S. Zou, G. C. Walker and M. Rubinstein, *Nat. Mater.*, 2007, **6**, 609–614.
46 Y. G. Sun and Y. N. Xia, *Science*, 2002, **298**, 2176–2179.
47 D. D. Lasic, P. M. Frederik, M. C. A. Stuart, Y. Barenholz and T. J. McIntosh, *FEBS Lett.*, 1992, **312**, 255–258.
48 S. Link, C. Burda, M. B. Mohamed, B. Nikoobakht and M. A. El-Sayed, *J. Phys. Chem. A*, 1999, **103**, 1165–1170.
49 E. Engel, R. Schraml, T. Maisch, K. Kobuch, B. Koenig, R. M. Szeimies, J. Hillenkamp, W. Baumler and R. Vasold, *Invest. Ophthalmol. Visual Sci.*, 2008, **49**, 1777–1783.
50 R. Vankayala, C. C. Lin, P. Kalluru, C. S. Chiang and K. C. Hwang, *Biomaterials*, 2014, **35**, 5527–5538.
51 W. Xiong, X. A. Gao, Y. B. Zhao, H. B. Xu and X. L. Yang, *Colloids Surf., B*, 2011, **84**, 103–110.
52 G. F. Zhou, Y. B. Zhao, J. D. Hu, L. Shen, W. Liu and X. L. Yang, *React. Funct. Polym.*, 2013, **73**, 1537–1543.

53 Y. Y. Ma, J. S. Wan, K. Qian, S. N. Geng, N. J. He, G. F. Zhou, Y. B. Zhao and X. L. Yang, *J. Mater. Chem. B*, 2014, **2**, 6044–6053.
54 D. K. Roper, W. Ahn and M. Hoepfner, *J. Phys. Chem. C*, 2007, **111**, 3636–3641.
55 C. M. Hessel, V. P. Pattani, M. Rasch, M. G. Panthani, B. Koo, J. W. Tunnell and B. A. Korgel, *Nano Lett.*, 2011, **11**, 2560–2566.
56 B. K. Wang, J. H. Wang, Q. Liu, H. Huang, M. Chen, K. Y. Li, C. Z. Li, X. F. Yu and P. K. Chu, *Biomaterials*, 2014, **35**, 1954–1966.
57 K. Qian, Y. Y. Ma, J. S. Wan, S. N. Geng, H. Li, Q. W. Fu, X. L. Peng, X. F. Kan, G. F. Zhou, W. Liu, B. Xiong, Y. B. Zhao, C. S. Zheng, X. L. Yang and H. B. Xu, *J. Controlled Release*, 2015, **212**, 41–49.
58 Y. B. Zhao, C. S. Zheng, Q. Wang, J. L. Fang, G. F. Zhou, H. Zhao, Y. J. Yang, H. B. Xu, G. S. Feng and X. L. Yang, *Adv. Funct. Mater.*, 2011, **21**, 2035–2042.
59 L. Y. Jiang, Q. Zhou, K. T. Mu, H. Xie, Y. H. Zhu, W. Z. Zhu, Y. B. Zhao, H. B. Xu and X. L. Yang, *Biomaterials*, 2013, **34**, 7418–7428.

Published on 02 tetor 2018. Downloaded by Fail Open on 7.5.2025 10:41:28 e paradites.

This journal is © The Royal Society of Chemistry 2018